Journal of Magnetics 17(2), 100-108 (2012) http://dx.doi.org/10.4283/JMAG.2012.17.2.100

Influence of Concentric Saddle Shaped Coils on the Behavior of a Permanent Magnet Transverse Flux Machine with Segmented Construction

Salwa Baserrah[1]*, Keno Rixen[2], and Bernd Orlik[1]

[1]*Institute of Power Electronics and Electric Drives, IALB, University of Bremen, Bremen, Germany*
[2]*Sciegra Research and Technologies GmbH, Hamburg, Germany*

(Received 9 November 2011, Received in final form 25 April 2012, Accepted 25 April 2012)

Flux concentrated permanent magnet transverse flux machines, FCPM-TFMs, with segmented stators require multi-turn concentric saddle coils to replace the ring coils, which are normally utilized in conventional layered-phase TFM constructions. In this paper, we investigate the influence of the shape of saddle phase windings and their parameter variations on the output torque productivity. Non-meshed coils evaluated via a finite element method (FEM) to examine the effect of the coil's location within one phase on machine performance. By using meshed coils, the analysis can be extended to inspect the distributions of magnetic field strength as well as current density in the coils. Throughout the study, the influence of design parameters on the output torque for two stator structures, i.e., a laminated and soft magnetic composite (SMC), are evaluated.

Keywords : segmented stator, saddle coils, transverse, design parameter, TFM, permanent magnet, SMC

1. Introduction

The maximum output power of flux concentrated permanent magnet machines, FCPM-TFMs, is limited by the temperature of the stator windings, which is mainly determined by the copper losses and the thermal resistance between the windings and the stator. Particularly, with segmented stator construction, additional copper losses arise due to the end windings located between the concentric saddle coils. The phases have been shown in [1] to work independently in a similar way to the conventional layered-phase construction.

Different winding configurations for the same stator lamination are compared in [2], with respect to the loss mechanisms and improvement of machine efficiency and maximum output power. This led to a new coil design that has improved the copper cross section area for switched reluctance machines. Superconducting coils with an inhomogeneous current density distribution yield more field for less volume of superconductor as described in [3, 4]. The inhomogeneous current field, which is produced by a set of concentric sub coils, shows a linear decrease with the radius of each sub coil. Although the aluminium coils appear to cost less than copper magnet systems, aluminium magnets should be avoided in high current density septum magnets, where the aluminium coils aggravate the heat transfer problems and when the magnet system is small, so a special cooling system is required [5]. A sensitivity analysis scheme for designing the shape of cylindrical probe coils that induce specified eddy current distributions inside the conducting cylinders was proposed in [6] based on Newton's optimization algorithm.

In this paper, the design of the phase windings of a rotational unsymmetrical FCPM-TFM, with segmented construction, is investigated through FEM utilizing the Flux3D software from Cedrat. The main design parameters of the windings are studied through implementing built-in non-meshed as well as designed meshed coils. For a given stator, the winding losses can be reduced by changing the layout of the stator windings; this study looks at two similar designs of the stator. Fig. 1 shows a three phase FCPM-TFM construction with special placement of the stator phases. The two stators being studied, laminated and pressed-SMC structures, are shown in Fig. 1(a) and Fig. 1(b), respectively. The main dimensions of the prototype FCPM-TFM with laminated-stator have already been presented in [7, 8], while the dimensions for the TFM with pressed-SMC are shown in Appendix 1.

*Corresponding author: Tel: +49(0)421-218 62689
Fax: +49(0)421-218 4318, e-mail: basurrah@ialb.uni-bremen.de

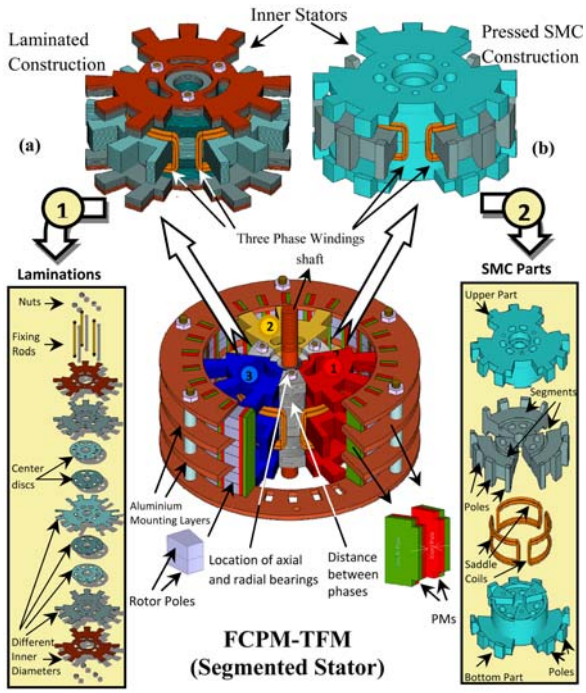

Fig. 1. (Color online) Permanent magnet transverse flux motor with sectors (a) Stator with laminations (b) Stator with SMC material.

2. Method of Analysis

Two similar constructions of the stators were designed; one in a laminated configuration and the other in a pressed configuration with soft magnetic composite (SMC) material, where the saddle windings are placed in the sectors around the stators. Both stators are of the same diameter, axial length and pole number and they undergo a comparison study through the use of three dimensional (3D)-FEM. Analytical study of the TFMs is performed with regard to the highest torque production capability and design parameter optimization for implementation of meshed coils conductors. The SMC material is from blanks of Somaloy Prototyping Material with an 80 mm diameter and 20 mm height. Non-oriented grain electric steel M270-50A is used in the laminated structure, which is isotropic, having the same mechanical and magnetic properties in all directions. This steel is often utilized in small electric motors. The BH-characteristics for both materials are shown in Fig. 2, where the Somaloy shows a lower saturation level.

2.1. Influence of design parameters on SMC stator

The design of the saddle coil is restricted by the available winding space. Therefore, the construction of the stator has to be optimized through varying different geometrical parameters. This study includes the SMC stator because SMC material is superior for torque production and because of its unique properties such as magnetic and thermal isotropy, very low eddy current loss and additionally because it is suitable for complex net shape manufacturing.

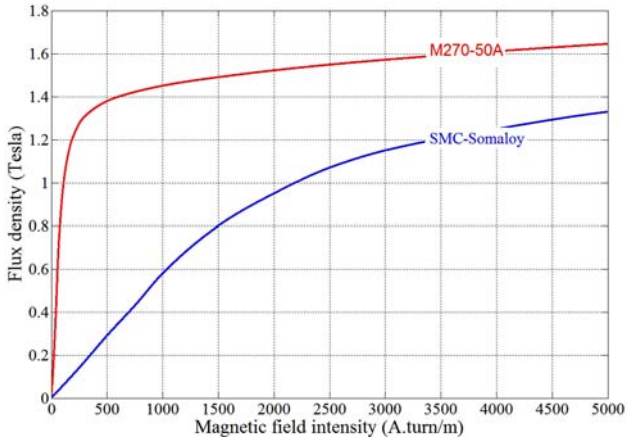

Fig. 2. (Color online) BH-curve of electric steel and SMC-Somaloy Magnetic field intensity (A.turn/m)

Furthermore, SMC material allows 3D-flux fields and facilitates the placement of windings packets through the pressed construction of the stator segments. Consequently, the effect of stator dimension parameters can be studied through the average output torque of the TFM with an SMC-constructed stator. The effect of the design parameters, illustrated in Fig. 3, on the 3D structure of the FCPM-TFM is investigated. These parameters include width and length variations of the stator pole and winding slot, the pole tip radial dimension and the tangential distance between the poles. The optimum design of the SMC construction is compared to the laminated construc-

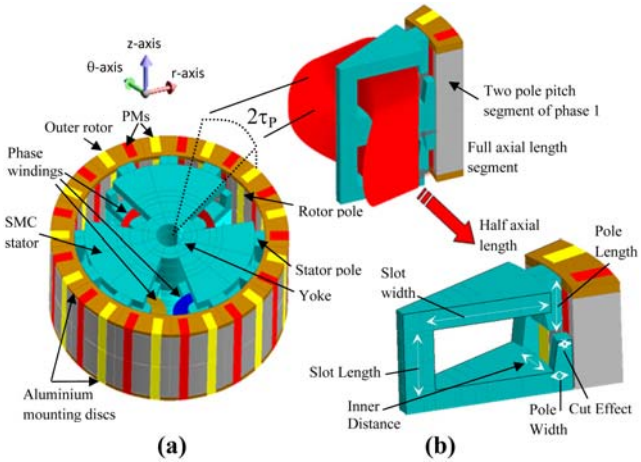

Fig. 3. (Color online) Assignment of design parameters for SMC stator (a) FCPM-TFM construction (b) Dimensions under study.

tion supplied with an adaptable current density of 4 A/mm^2 and a high fill factor. Basically, the comparison criterion is the impact of the stator material on different components of the output torque of the machine. An increase of the effective area of the stator poles that faces the air gap via use of the SMC material, leads to a significant improvement in the torque. Unfortunately, this pole shaping cannot be achieved in the laminated structure.

2.2. Non-meshed coils via magneto-static analysis

Non-meshed coils can be simulated via Flux3D using a reduced magnetic scalar potential. These coils are geometric entities of different shapes, which are superimposed onto the mesh but have no dependence on it. Fig. 4 shows a detailed description of the saddle shaped coils simple placement method for the SMC stator and the required dimensions for each coil, these are then studied and optimized. The top and bottom parts carry the axial and radial bearings of the machine. The studied dimensions of the saddle phase coils are found in Table 1 and shown in Fig. 4(b), where they are wound over a two pole pitch, $2\tau_p$, segment of the stator. The central field, B_o, of the saddle coil is normally given by [9]:

$$B_o = (4\vec{i}/\pi)\mu_o \cdot N \cdot I(h_m/D^2) \cdot (s^{-0.5} + s^{-1.5}) \cdot \sin(\alpha/2) \quad (1)$$

where $\vec{i}$ is the unit vector in a direction perpendicular to the coil plane, I is current in the coil and $s = 1 + (h_m/D)^2$, D is the diameter and h_m is the mean axial length of the saddle coil as shown in Fig. 4(b).

No second order field derivatives, in any direction, exist for saddle coils when the length-to-diameter ratio is equal to two and the circular arcs span 120°. The field in space, which is calculated by the Biot-Savart law, is expressed as a power series involving derivatives of the field with respect to r, θ, and z evaluated at the centre of the coil system. For compatible settings of angles and heights of the coil, certain restrictions are imposed. These restrictions are shown in (2) and (3).

Table 1. Saddle coil dimensions.

Opening angle of straight part, φ (°)	15
Opening angle of cylindrical part, Ψ (°)	73
Length of straight part of saddle coil, l (mm)	7
Internal half height of saddle coil, h (mm)	6.7
Radius of cylinder of saddle, R (mm)	25.3
Total angle of saddle, α (°)	$9.3 \times \tau_p$
Number of turns per saddle coil , N	9

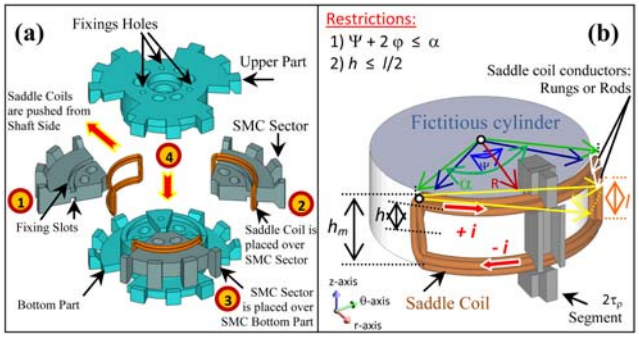

Fig. 4. (Color online) Placement of saddle coils on phase sectors (a) Placement of saddle coils (b) Dimensions of coil.

$$\Psi + 2\varphi \le \alpha \quad (2)$$

$$h \le l/2 \quad (3)$$

The general form of equation solved in the scalar model by FEM in magneto-static application is given by (4).

$$\mathrm{div}([\mu_r]\mu_o(-\mathrm{grad}(\phi) + \vec{T}) + \vec{B}_r) \quad (4)$$

where μ_r and μ_o are the tensor of the relative permeability of the medium and the permeability of a vacuum, respectively. ϕ is a magnetic scalar potential in Ampere $\vec{T}$ corresponding to sources in A/m, $\vec{B}_r$ is the remanent magnetic flux vector in Tesla. In the case of a non-meshed current source,

$$\vec{T} = \vec{H}_j \quad (5)$$

where, $\vec{H}_j$ is the magnetic field created by a non-meshed coil.

$$\phi = \phi_{\mathrm{red}\ H_j} \quad (6)$$

The state variable for the non meshed coil is $\phi_{\mathrm{red}\ H_j}$ and the magnetic field strength, $\vec{H}$ is given by:

$$\vec{H} = -\mathrm{grad}\,\phi_{\mathrm{red}\ H_j} + \vec{H}_j \quad (7)$$

By substituting (5), (6) into (4) we get:

$$\mathrm{div}([\mu_r]\mu_o(-\mathrm{grad}(\phi_{\mathrm{red}\ H_j} + \vec{H}_j)) + \vec{B}_r) \quad (8)$$

The computation of the magnetic field intensity, $\vec{H}$, of the non-meshed coil created by the current distribution is carried out using Biot-Savart law in an analytic or semi-analytic way [10].

2.3. Meshed coils via magneto-static analysis

Meshed coils utilize the reduced magnetic scalar potential

with respect to uniform current density in the meshed region of the field sources. Therefore, for the case of meshed coils,

$$\vec{H} = \vec{T}_o \tag{9}$$

and $\vec{T}_o$ is the electric vector potential and satisfies (10).

$$\text{curl}(\vec{T}_o) = \vec{J}_s \tag{10}$$

where $\vec{J}_s$ is the current density in the meshed region of the field source and the scalar magnetic potential is as it is in (11).

$$\phi = \phi_{\text{red } T_o} \tag{11}$$

Thus, the magnetic field intensity, $\vec{H}$ of the meshed coil is given by (12).

$$\vec{H} = -\text{grad}\,\phi_{\text{red } T_o} + \vec{T}_o \tag{12}$$

By substituting (9) and (11) into (4), the resulting equation for the meshed coil case is (13).

$$\text{div}([\mu_r]\mu_o(-\text{grad}(\phi_{\text{red } T_o} + \vec{T}_o)) + \vec{B}_r) \tag{13}$$

For the meshed coils, (13) will be solved and the state variables are $\phi_{\text{red } T_o}$ and $\vec{T}_o$ are found.

It should be pointed out that a domain can contain meshed and non-meshed coils at the same time. Therefore, equation (10) changes to (14).

$$\text{curl}(\vec{T}_o) = \vec{J}_s + \text{curl}(\vec{H}_j) \tag{14}$$

where $\vec{J}_s$ corresponds to meshed conductors and $\text{curl}(\vec{H}_j)$ to the field created by non-meshed coils.

Computation of the Laplace force, $\vec{F}_L$ can be performed by only using meshed conductors and is expressed by (15).

$$\vec{F}_L = \int_v \vec{J}_s \times \vec{B}\, dv \tag{15}$$

3. Results and Analysis

The magneto-static study conducted by FEM is divided into two sections, where at the beginning, the influence of the variations of certain geometrical design parameters of the SMC constructed stator are studied. Next, non-meshed and meshed coils were designed and the variations of their dimensions were studied too. Throughout the study, the most suitable design for the winding scheme was pursued, where the current density and fill factor of the coils are taken into account.

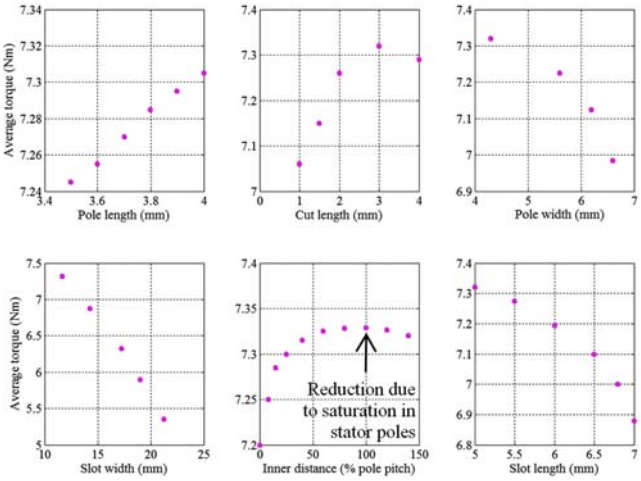

Fig. 5. (Color online) Influence of parameters variations on average torque.

3.1. Influence of design parameters

The effects of the variations of the parameters for the SMC built stator on the average torque of a three-phase FCPM-TFM are depicted in Fig. 5. A stator with a pole length and width of 4.0 mm and 4.3 mm, respectively, and a pole cut of 3.0 mm give the highest average torque when the distance between the stator poles is kept within a certain interval [100% τ_P, 120% τ_P]. Fig. 6 shows the cogging, reluctance and interaction torque components of the optimal SMC construction obtained after a design parametric study with a sinusoidal current supply [11].

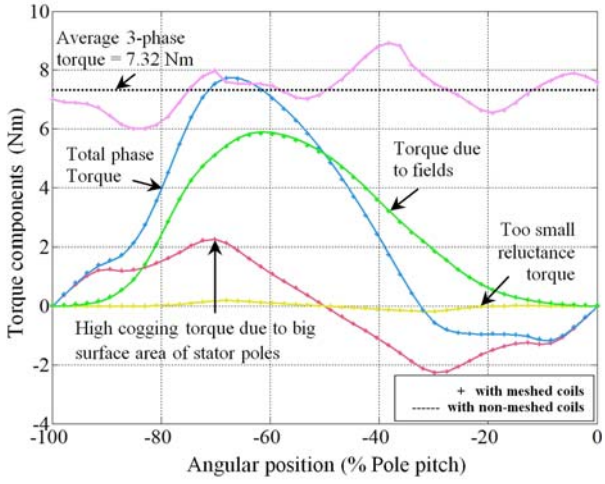

Fig. 6. (Color online) Torque components of TFM with SMC stator.

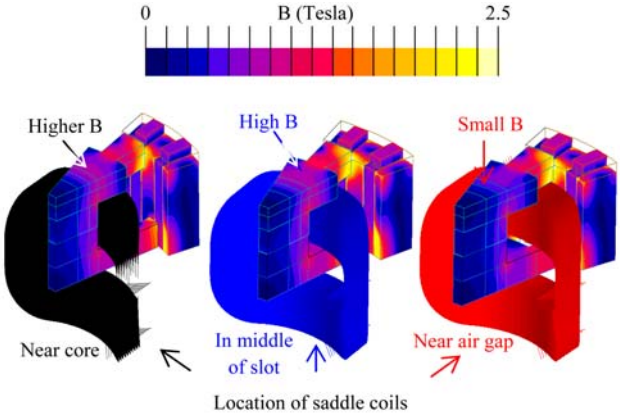

Fig. 7. (Color online) Effect of location of saddle coils on flux density.

Obviously, SMC shows a high cogging torque compared to reluctance torque.

3.2. Effect of non-meshed saddle coils

Through utilization of non-meshed coils, the induced flux and flux linkage in the coils due to PMs and armature current can be studied, this was already investigated in [12-14].

Ten saddle coils with 10 turns are placed into the available slots; each turn has a 1.0 mm^2 cross section area. The dimensions of the coils are set according to Table 1. Three cases were studied: 1) The coils are moved towards the core, 2) The coils are placed in the middle of the slot and 3) The coils are shifted toward the poles. The influence of the location of the coils on the flux density and the induced flux in the coils was studied, as the results can be seen in Fig. 7 and Fig. 8, respectively. The distributions of the flux density modulus for the laminated

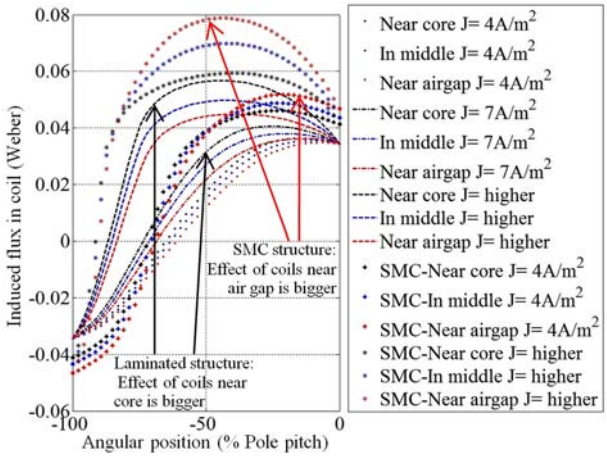

Fig. 8. (Color online) Impact of location of saddle coils on induced flux (for different current densities).

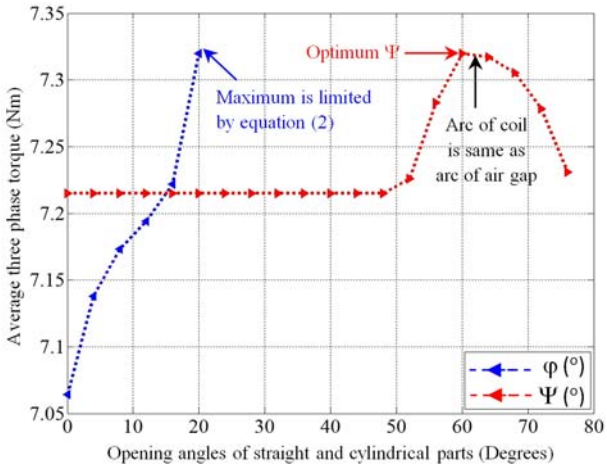

Fig. 9. (Color online) Effect of opening angles of coils on average torque.

stator with the rotor at the non-aligned position are shown in Fig. 7, where the peak value of the current source is applied. The places in the stator occupied by the coils will show higher values of flux density.

For the laminated stator case, the induced flux in the phase coils will be higher if the coils are placed near the core. The increase in flux was recorded to be 33.3% at the q-axis position; this can be seen in Fig. 8 for different current densities. However, this case shows opposite behavior to that of the SMC stator. For the SMC stator the location of coils should not be close to the air gap due to the increased surface areas of the poles, this will initiate the pole tip effect that causes the stray flux that, in turn, will increase the eddy current losses of the coil conductors. Note that the induced fluxes are shown to display the total effect from the PMs and armature currents.

The effects of the dimensions of the saddle coils are shown in Fig. 9, where the effect of the opening angles of the straight part and the cylindrical part, Ψ and φ, respectively, are shown. They show slight effects on the average torque. The angle of the cylindrical part, Ψ has an optimum value, thereafter the output torque reduces; whereas the angle of the straight part, φ is directly proportional to the output average torque.

3.3. Effect of meshed saddle coils

The meshed coil principle allows the study of the magnetic field strength in the winding. It is being calculated by Flux3D via equation (12). Appendix 2 shows how to simulate a meshed coil via Flux3D. The volume of the coil is set as the coil conductor region with a specified current density of 4 A/mm^2 and an optimum fill factor. Fig. 10(a) illustrates the current terminals and the meshed elements of the coil region, which is meshed with ≈ 336000

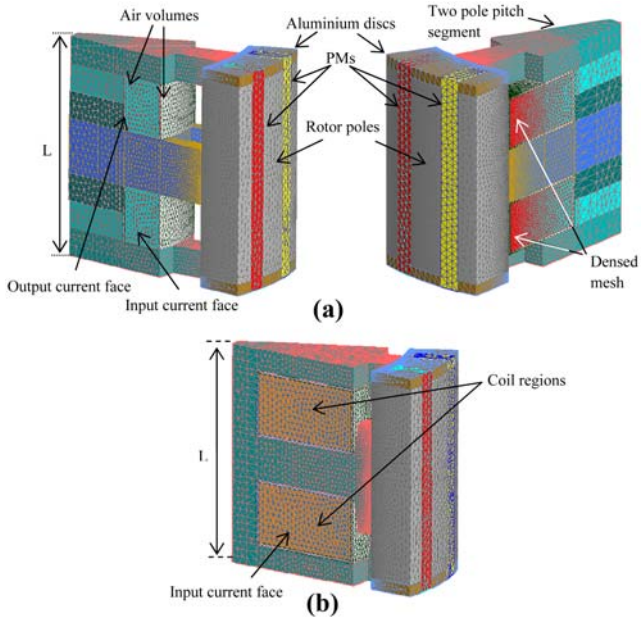

Fig. 10. (Color online) Location of meshed coils in $2\tau_p$ of TFM (a) Laminated stator (b) SMC stator

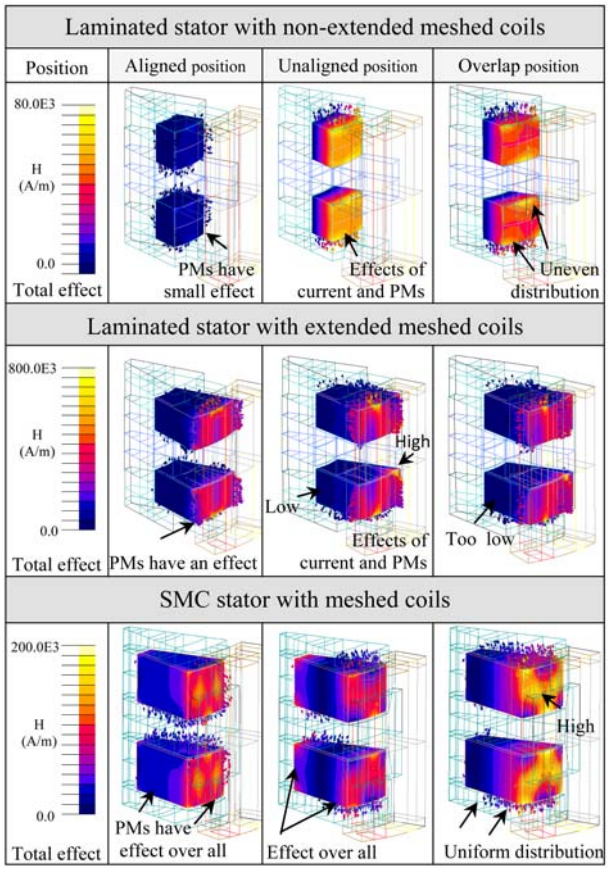

Fig. 11. (Color online) Distribution of magnetic field strength, H (A.turn/m).

and ≈ 438000 second order mesh elements for non-extended and extended designs of the laminated constructed stator. The corresponding construction of SMC material is shown in Fig. 10(b) with ≈ 343000 second order elements for a full slot winding design.

Fig. 11 demonstrates the magnetic field strength of the coil for three locations of the rotor, i.e., aligned, unaligned and overlap, for 3 kinds of load condition:

1) Laminated with non-extended coils
2) Laminated with extended coils
3) SMC stator with full slot coils

The applied current is of a sinusoidal waveform. The magnetic field strength in the first case for all the positions appears to be smallest compared to the other two cases. This is due to the assigned number of turns 100, 200 and 300 for the three cases, respectively.

The effect of the field of the PMs can be seen at the aligned position where the current is zero. To illustrate the current density distribution of the coil, magneto-static cannot be used, since uniform current density is assumed in this application.

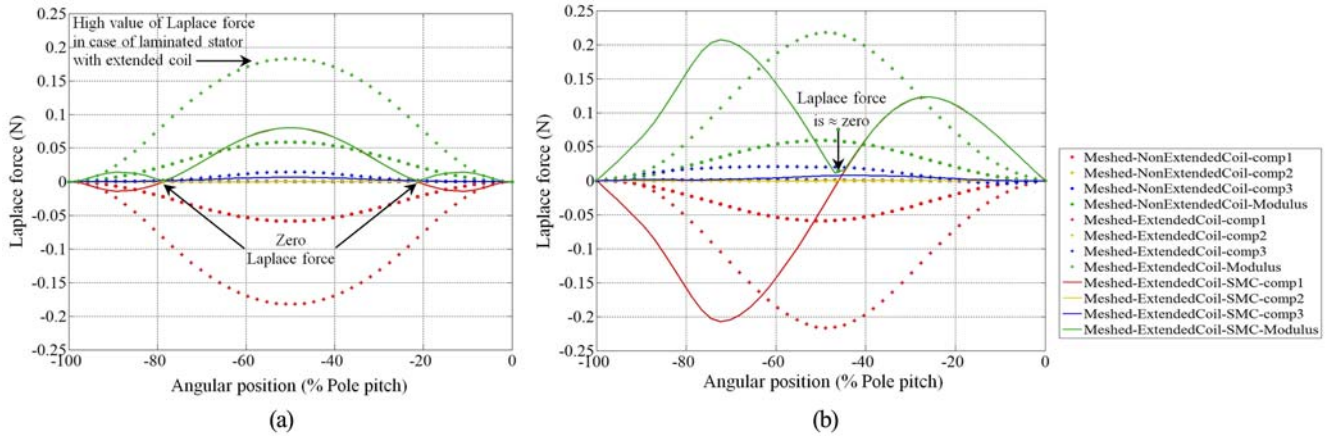

Fig. 12. (Color online) Laplace force exerted on meshed coil (a) Effect of current only (b) Total effect.

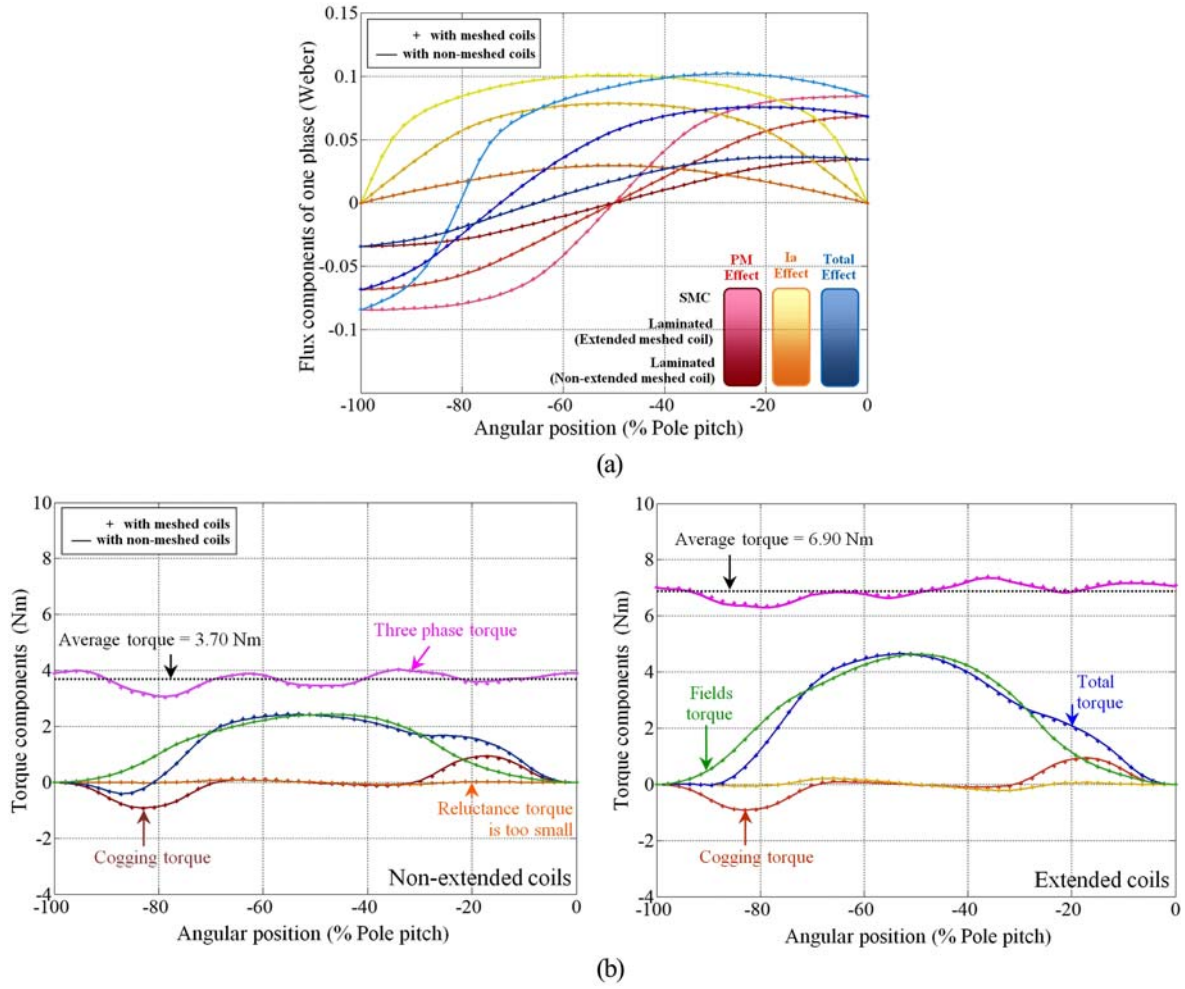

Fig. 13. (Color online) Comparison between meshed and non meshed coil (a) Induced flux (b) Torque components.

Therefore, transient analysis solves this problem by introducing a solid conducting region for the coil, where a current source is connected, either in a virtual way or through connecting an electric circuit. The assigned value of the current source should account for the total Ampere-turn of the source. Appendix 3 shows the circular current paths in the coil region in a transient state, where they concentrate on the surface of the coil.

In the case of meshed type coils, the value of the current source is provided at all points of the coil; therefore, the computation of the Laplace force is achievable, while in non-meshed coils computing the Laplace force is not directly possible. Fig. 12 shows the Laplace force that is exerted on one side of a current carrying conductor placed on the magnetic field for two cases: when PMs are removed and when both armature currents and PMs exist. The laminated stator with extended meshed coil shows the highest magnetic field intensity. Uniform magnetic field strength is recorded for the SMC constructed stator. The magnetic field intensity is affected by the fill factor and current density of the winding. The radial component is dominant in all cases and it reduces to zero for more than one position of the SMC stator.

Fig. 13(a) shows the fluxes induced in the phase coils obtained by using meshed and non-meshed simulations for the three studied cases. Under load condition, the fluxes in the coils are produced from PMs and armature currents. The individual components of the flux are calculated by using the frozen permeability technique [15]. Note that the phases of the induced fluxes are not the same. Fig. 13(b) shows the torque components for non-extended and extended coil cases. The output torque from TFM of the stator with an extended coil shows an increase of 86.5% compared to the non-extended coil, while the other torque components are small.

Implementing an electric circuit in Flux3D facilitates getting the voltage out of the coils through post-processing and it also allows the user to define the source as a

Table 2. Local and global quantities in FLUX3D (for non-meshed and meshed coils) [10]

3D-Application	Type of Coil	
	Non-meshed coil	Meshed coil
Magneto-static/ Transient/Steady state AC magnetic	Local Quantities	
	$\vec{H}_j$	$\vec{H}$, $\vec{J}_s^*$, $d\vec{F}_L$
	Global Quantities	
	Φ_b	Φ_b, $\vec{F}_L$

*Uniform in case of Magneto-static and non-uniform in case of Transient/Steady state AC magnetic applications

voltage source, however, it is by default used as a current source. Using solid conductor regions takes into account the skin effects as well as the non-uniformity of the current density, which cannot be considered in the case of the coil conductor regions. By linking the regions of coil or solid conductors of the FE- domain to their correspondence to the associated electric circuit, coupling is achieved. Moreover the wiring parameters such as the resistance and inductance can be specified too. The electric circuit can be applied through transient analysis and 3D steady state AC magnetic schemes. Table 2 shows a summary of the local and global quantities for the non-meshed and meshed coils, which can be calculated specifically in magneto-static, transient and steady state AC magnetic applications of the software.

4. Conclusion

An optimum design of saddle coil can be achieved through studying different design parameters related to the windings and the stator constructions. Utilizing the meshed coil regions, many aspects of the design can be studied, such as the influence of coil dimensions, the magnetic field strength and the Laplace force, which are difficult to be obtained when the study domain involves non-meshed coils. However, the main advantage of the non-meshed coils is the reduction of the number of nodes and the fact they can be defined before and after mesh execution, whereas the accuracy of the results in meshed conductors depends on how fine the mesh is, and in particular on the mesh around the coils.

Since the winding and slot having an interactive effect; an SMC constructed stator was optimized and compared to a laminated stator. The SMC construction shows better utilization of the slot space, in addition to an easy proposed windings placement method and manufacturing process. SMC has achieved ≈ 6% increase in average torque compare to the laminated design with extended coil for the same current density. Moreover, the locations of coils in the slot show different induced flux variations for both constructions of the stator.

Appendix 1

Main dimensions (in mm) of $2\tau_p$ segment of SMC stator*

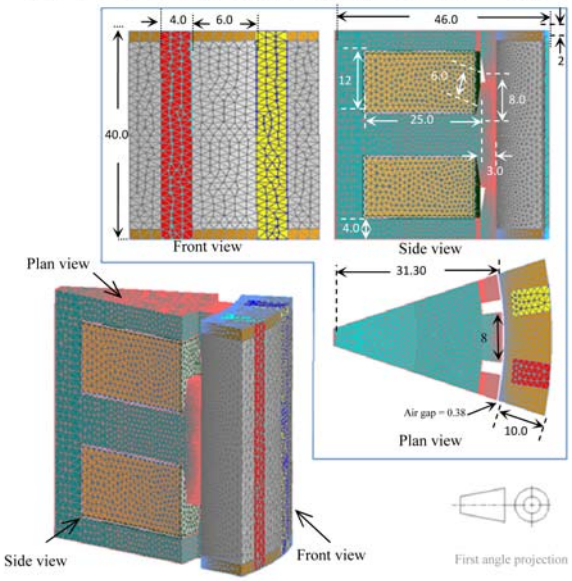

*Dimensions of FCPM-TFM with laminated stator can be found in [7], [8].

Appendix 2

(Principle of open and closed coils)

The constructing of 3D meshed open coils requires the following aspects to be fulfilling for proper operation:

- The same shape for entering and exiting faces of the current,
- The number of lines connecting entering and exiting faces of the current should be the same,
- Air volumes must be placed around the meshed coil region. If these are not defined, the coil conductor region will not consider the assigned current.

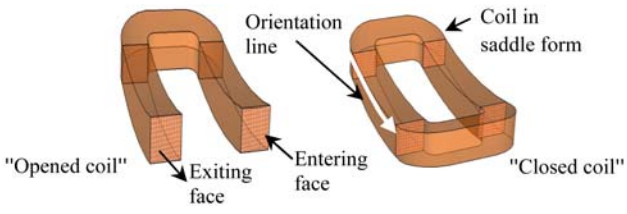

Appendix 3

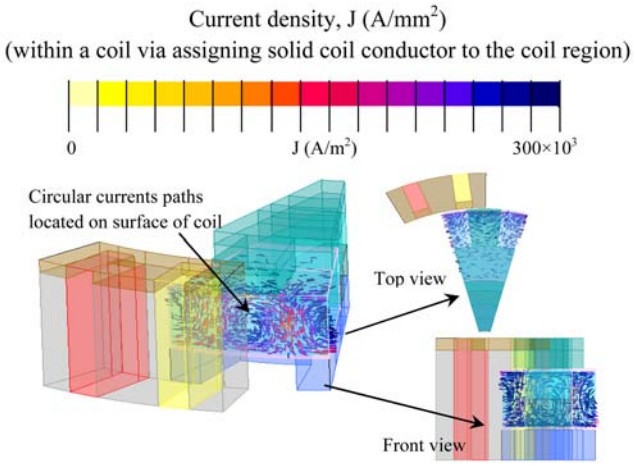

References

[1] S. Baserrah, K. Rixen, and B. Orlik, Proc. IEEE International Conf. on Power Electronics and Drive Systems 102 (2009).
[2] C. E. Carstensen, S. E. Bauer, R B. Inderka, and R. De Doncker, Proceedings of 20th International Electric Vehicle Symposium (2003).
[3] H. Burkhard, J. Phys.: Appl. Phys. **6**, 357 (1975).
[4] G. Drago, P. Molfino, M. Repetto, G. Secondo, G. M. A. Lia, and P. L. Ribani, IEEE Trans. Magn. **28**, 450 (1992).
[5] M. A. Green, IEEE Trans. Nuclear Science **14**, 398 (1967).
[6] I. T. Rekanos, C. S. Antonopoulos, and T. D. Tsiboukis, IEEE Trans. Magn. **35**, 1797 (1999).
[7] S. Baserrah, K. Rixen, and B. Orlik, Proceedings of PCIM 2010, 580 (2010).
[8] S. Baserrah, K. Rixen, and B. Orlik, Proceedings of PCIM 2010, 65 (2010).
[9] D. M. Ginsberg and M. J. Melchner, Review of Scientific Instruments **41**, 122 (1970).
[10] User's Guide of Flux Software **3**, 48 (2009).
[11] S. Baserrah and B. Orlik, IEEE International Conf. on Power Electronics and Drive Systems 96 (2009).
[12] S. Baserrah, K. Rixen, and B. Orlik, Proc. International Conf. Electrical Machines and Systems 963 (2010).
[13] S. Baserrah, K. Rixen, and B. Orlik, J. Electrical Engineering and Technology **7**, 184 (2012).
[14] S. Baserrah and B. Orlik, Proc. IEEE-IEMDC 630 (2011).
[15] J. A. Walker, D. G. Dorrell, and C. Cossar, IEEE Trans. Magn. **41**, 3946 (2005).